Journal Pre-proof

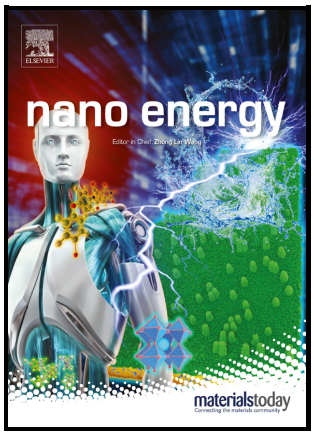

Highly Permeable and Ultrastretchable E-Textiles with EGaIn-Superlyophilicity for On-Skin Health Monitoring, Joule Heating, and Electromagnetic Shielding

Jiancheng Dong, Xinwei Tang, Yidong Peng, Chonghui Fan, Le Li, Chao Zhang, Feili Lai, Guanjie He, Piming Ma, Zicheng Wang, Qufu Wei, Xiu-Ping Yan, Hai-Long Qian, Yunpeng Huang, Tianxi Liu

PII: S2211-2855(23)00030-7

DOI: https://doi.org/10.1016/j.nanoen.2023.108194

Reference: NANOEN108194

To appear in: *Nano Energy*

Received date: 24 October 2022
Revised date: 30 December 2022
Accepted date: 6 January 2023

Please cite this article as: Jiancheng Dong, Xinwei Tang, Yidong Peng, Chonghui Fan, Le Li, Chao Zhang, Feili Lai, Guanjie He, Piming Ma, Zicheng Wang, Qufu Wei, Xiu-Ping Yan, Hai-Long Qian, Yunpeng Huang and Tianxi Liu, Highly Permeable and Ultrastretchable E-Textiles with EGaIn-Superlyophilicity for On-Skin Health Monitoring, Joule Heating, and Electromagnetic Shielding , *Nano Energy,* (2022) doi:https://doi.org/10.1016/j.nanoen.2023.108194

Highly Permeable and Ultrastretchable E-Textiles with EGaIn-Superlyophilicity for On-Skin Health Monitoring, Joule Heating, and Electromagnetic Shielding

Jiancheng Dong[a], Xinwei Tang[a], Yidong Peng[a], Chonghui Fan[b], Le Li[a], Chao Zhang[c], Feili Lai[d,e], Guanjie He[f], Piming Ma[a], Zicheng Wang[a], Qufu Wei[b], Xiu-Ping Yan[g], Hai-Long Qian[g], Yunpeng Huang[a,*], Tianxi Liu[a,*]

[a] Key Laboratory of Synthetic and Biological Colloids, Ministry of Education, School of Chemical and Material Engineering, Jiangnan University, Wuxi, 214122, China

[b] Key Laboratory of Eco-Textiles, Ministry of Education, Jiangnan University, Wuxi, 214122, China

[c] State Key Laboratory for Modification of Chemical Fibers and Polymer Materials, College of Materials Science and Engineering, Donghua University, Shanghai, 201620, China

[d] Department of Chemistry, KU Leuven, Celestijnenlaan 200F, Leuven 3001, Belgium

[e] Department of Molecular Spectroscopy, Max Planck Institute for Polymer Research, Ackermannweg 10, 55128 Mainz, Germany

[f] Christopher Ingold Laboratory, Department of Chemistry, University College London, 20 Gordon Street, London WC1H 0AJ, UK

[g] School of Food Science and Technology, Jiangnan University, Wuxi 214122, China

*** Corresponding authors**

E-mail: hypjnu@jiangnan.edu.cn (Y. P. Huang), txliu@jiangnan.edu.cn (T. X. Liu)

Abstract

The prosperity of wearable and healthcare electronics yearns for the compact integration of multi-functionalities including detectability for various electrophysiological signals, thermal/moisture management, and electromagnetic wave protection. Herein, highly breathable and ultrastretchable styrene-ethylene-butylene-styrene (SEBS)-Ag-liquid metal (SSLM) nonwoven electronic textiles are fabricated as versatile on-skin bioelectrodes for accurate health monitoring, Joule heating, and electromagnetic interface (EMI) shielding. Taking advantage of the reactive alloying between liquid metal and magnetron sputtered

silver nanoparticles, ultra-conductive eutectic gallium-indium (EGaIn) is intimately and uniformly encapsulated on superlyophilic SEBS microfibers after activation via monolithic pre-stretching. Benefiting from the highly deformable, extremely stable, and 3D interconnected conducting networks, the nonwoven E-textiles demonstrate exceptional EMI shielding effectiveness (75.3 dB at frequencies of 8.2-12.8 GHz, and still maintain 31.7 dB at 300% elongation), and efficient Joule heating performance also under large-scale deformation (120%). Moreover, the breathable SSLM E-textiles used as skin-attachable bioelectrodes even manifest prominent monitoring performance for biophysical signals (breath, phonation, and joint bending), surface electromyography signals (sEMG), and electroencephalogram signals (EEG). Therefore, the superlyophilicity and superior performance of the liquid metal E-textiles enable a wide range of applications in next-generation skin electronics and protective textiles.

Keywords

electronic textiles, on-skin bioelectrodes, liquid metals, human health regulation, Joule heaters, electromagnetic interface shielding

1. Introduction

Portable and stretchable electronic technologies have tremendous application prospects in artificial skin [1-3], metaverse interfacing [4,5], internet of things (IoT) [6,7], and energy storage technologies [8-10]. Amongst, skin attachable electrodes with characteristics including high electric conductivity, superior stretchability, great permeability as well as long-term wearing comfort hold enormous potential in health care industries [11-13]. However, the electromagnetic waves generated by chips and circuits not only significantly affect the performance of wearable electronics but also threaten human health, especially for pregnant women [14-18]. Thus, on-skin devices with remarkable electromagnetic interference (EMI) shielding capability are highly favorable for their practical applications [19]. Additionally, it is widely acknowledged that the high and stable electrical conductivity of an on-skin device is crucial for both the EMI shielding efficacy and the high-fidelity recording of human electrophysiological signals [20-23]. Conventional conductive materials

including various metal nanomaterials (e.g., silver nanoparticles and silver nanowires) [24-27], carbonaceous materials (such as carbon foam and graphene) [28,29], and transition-metal carbonitrides [30-33] always suffer from high density, inferior stability, and poor flexibility, which cannot simultaneously satisfy the requirements of lightweight, permeability, elasticity, and lengthy durability.

Liquid metal (LM, such as eutectic gallium-indium) is a class of promising conducting materials featuring infinite deformability, excellent recyclability, great self-healability, and remarkable biocompatibility, which can maintain their superior conductivity (>3×10^4 S cm^{-1}) under ultra-large strains [34-36]. In addition, the easy printing of LM on various substrates also provides a promising solution for the large-scale and low-cost manufacturing of stretchable electronics. As yet, the low wettability and poor affinity between LM and polymeric substrates are still major challenges hindering the advancement of LM in stretchable electronics due to its high surface tension (~700 mN m^{-1}) [37,38]. Previous works endeavored to enhance the wettability of LM through encapsulating LM microdroplets within hydrophilic polymers (e.g., polysaccharide, PVP, and PEO) [39-41], yet such approaches inevitably induced insulative junctions among the LM particles, thus largely decreased the conductivity of the conductor as a consequence. Other approaches tried to wet the LM with metal flakes or acid vapor to improve the binding force between elastic matrixes and LM. For instance, Ag nanoparticles were chemically reduced on the stretchable substrate to successfully increase the loading amount and lyophilicity of LM on elastomeric fibers. Nevertheless, the utilization of a virulent reductant (hydrazine) was not suitable for skin-attaching applications [42]. Another research work applied HCl vapor and microstructured copper-enhanced surfaces to completely wet the eutectic gallium-indium [43], yet the harmful acid vapor and limited LM loading capacity cannot meet the demands for epidermal electronics. Apart from these, most of the previously reported flexible on-skin electronics were constructed on hermetical matrixes (casted TPU, PDMS, and PI film) [44,45], long-term wearing of the impermeable electronics would cause skin irritation,

allergy, and even inflammation, thus fail to meet the rigorous requirements of long-term wearing comfort.

In this research, an ultrastretchable and highly permeable liquid metal E-textile was developed as multifunctional on-skin electrode for EMI shielding, Joule heating, and personal health monitoring. To start with, supremely porous electrospun styrene-ethylene-butylene-styrene (SEBS) nonwoven textile was magnetic-sputtered with a thin, compact, and uniform nano-Ag layer, thus facilitating the homogeneous and intimate coating of ultra-highly conductive LM on individual SEBS microfibers owing to the fast alloying of EGaIn with Ag NPs. Obtained SEBS-Ag-LM (SSLM) E-textile was eventually activated via pre-stretching to realize the ultra-stretchable, 3D interconnected, and highly permeable conducting networks. As a consequence, the SSLM E-textiles show superior EMI shielding effectiveness up to 75.3 dB at frequencies from 8.2 GHz to 12.8 GHz, more excitingly, this metamaterial can satisfy commercial shielding requirements (>30 dB) even at strain up to 300%. Besides, the construction of consecutive LM networks endowed the SSLM textile with efficient electro-thermal generation, and precise health monitoring capability including breath, phonation, surface electromyography (sEMG), and even electroencephalogram (EEG) signals. Therefore, this all-rounded SSLM E-textile is supremely valuable for wearable health regulation devices integrated with EMI shielding capabilities.

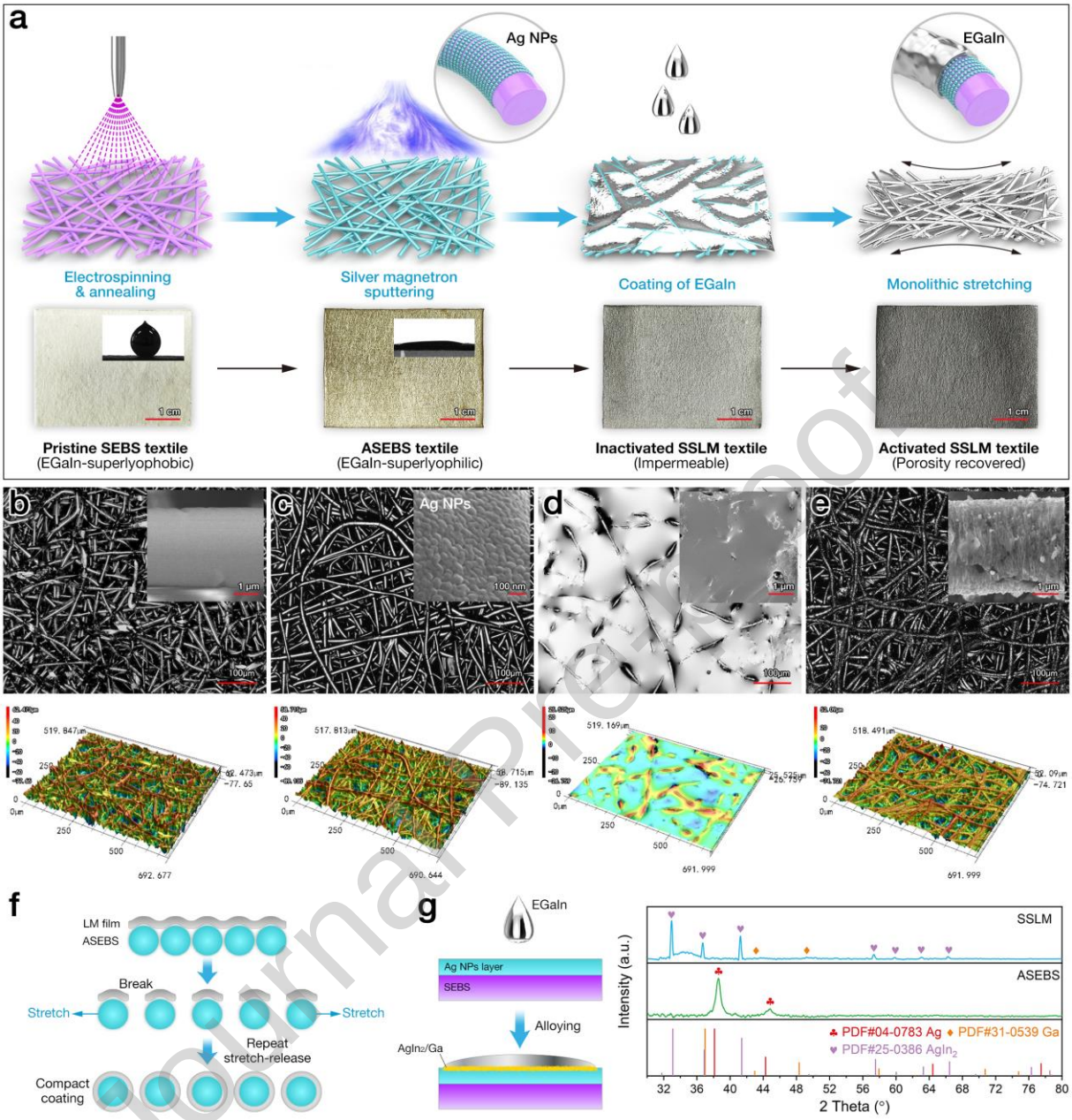

Figure 1. (a) Fabrication process of the highly conductive and permeable SSLM E-textiles, and corresponding digital photographs of samples obtained at each step. Laser microscopic images, SEM images, and corresponding 3D surface topographic images of (b) pristine SEBS fiber substrates, (c) ASEBS textile, (d) inactivated SSLM textile, and (e) activated SSLM E-textile. (f) Activation process of SSLM E-textile via monolithic stretching. (g) The wetting mechanism of EGaIn on Ag NPs incorporated fibers, and the XRD patterns of ASEBS and SSLM textiles.

2. Results and Discussion

2.1. Design and Fabrication of SSLM E-Textiles

The fabrication process of the SSLM E-textile is schematically shown in Figure 1a, free-standing SEBS nonwoven was first prepared through electrospinning, which exhibited poor LM affinity with a contact angle (CA) of ~143.4° (inset of **Figure 1**a). Obtained microfibers exhibited a highly porous structure and smooth surface as revealed in SEM images and laser microscopic images (Figure 1b). The mean diameter and the average pore size of pristine SEBS microfibers were measured to be 8.13 μm and 13.47 μm, respectively (Figure S1). The white nonwoven textile turned out to be a pale golden appearance after silver magnetic sputtering (inset of Figure 1a). Meanwhile, the microfibers perfectly maintained the uniform and highly porous morphology (Figure 1c). Further EDS mapping and high-resolution SEM observation indicate the Ag nanoparticles were evenly distributed with a size of ~50 nm (Figure S2, inset of Figure 1c), and the Ag loading amount was approximately 21.6 wt.%. Interestingly, the CA of LM on the Ag-sputtered SEBS textile (ASEBS) dramatically decreased to ~8°, proving the superlyophilicity of the nanosilver layer towards Gallium–Indium eutectic. As a consequence, ultrastretchable electronic textiles were subsequently fabricated via coating LM onto the ASEBS microfibers. The LM with great fluidity could spread and infuse into the microporous ASEBS nonwoven through the capillary force. Clearly, the porous structure of the microfibers was completely covered and filled by the shining grey LM, on which a continuous and impermeable layer of liquid metal lay on the surface (Figure 1d), potentially deteriorating the long-term perspiration process when applied as on-skin electronics.

Concerning the above issues, a simple pre-stretching strategy was used to recover the 3D interconnected porosity in the nonwoven textile (Figure 1f) [13]. As demonstrated in Figure 1e, after activation via 3-5 cycles of mild stretching (~500%), the continuous LM bulk film on the textile transformed to a mesh-like morphology that resembled the pristine SEBS matrix. The laser image reveals that the EGaIn was compactly and uniformly coated onto individual microfibers, maintaining highly permeable and conductive networks to ensure

stable/fast charge transfer and comfort wearing as on-skin electronics. The excellent wetting and integration of EGaIn with ASEBS textile could be explained by the reactive alloying between Ag and LM (Figure 1g). Previous research has successfully developed biphasic liquid metal composites involving EGaIn and Ag flakes, achieves desirable conductivity and printability [46]. Similarly in this work, the well-defined characteristic peaks in the XRD patterns prove the deposition of EGaIn on the surface of Ag NPs initiates the formation of $AgIn_2$ (PDF#25-0386) and Ga phases, leading to the superlyophilic surface of ASEBS fiber matrixes. Meanwhile, microscale wrinkles formed on the pre-stretched LM-encapsulated fibers possess a prolonged conductive pathway (inset of Figure 1e), which is highly beneficial for maintaining high conductivity under large strains [47]. The EDS mapping further proves that Ga, In, O (from Ga_2O_3) [48], and Ag elements were evenly distributed on the surface of the SSLM fibers (Figure S3). Water moisture permeability tests on the samples showed that there was a 43.79% loss of permeability on un-stretched SSLM, decreasing from 1965.21 g m^{-2} day^{-1} (ASEBS) to 1104.56 g m^{-2} day^{-1}. Whereas the pre-stretch activated SSLM showed neglectable permeability loss (1824.34 g m^{-2} day^{-1}) as shown in Figure S4.

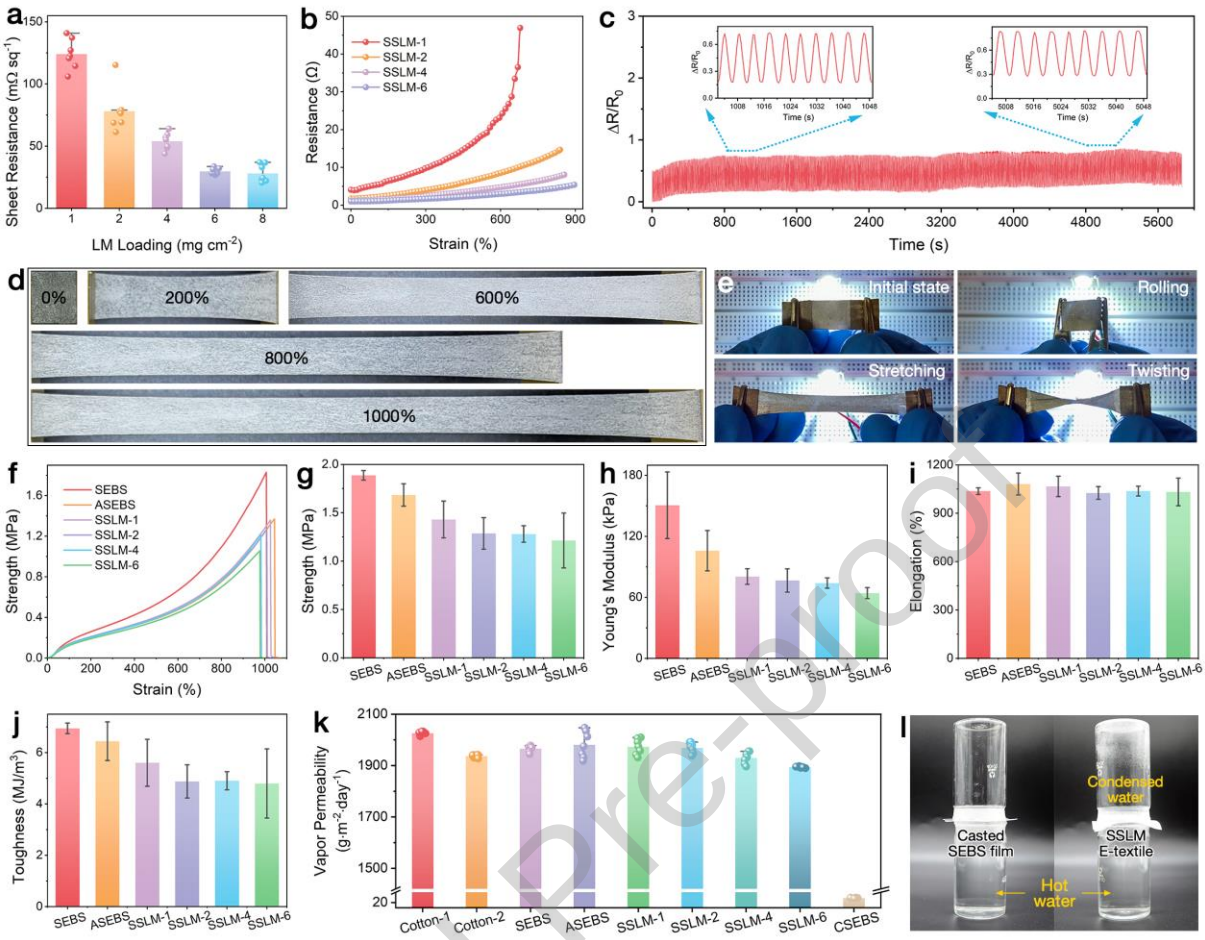

Figure 2. (a) Sheet resistance and (b) resistance versus strains of SSLM textile with different EGaIn loadings. (c) Resistance changes of SSLM during 1000 successive tensile cycles at 100% strain. (d) Digital photos of the SSLM E-textiles at strains of 0%, 200%, 600%, 800%, and 1000%. (e) Electrical conductivity of the SSLM E-textiles under stretching, rolling, and extreme twisting. (f-j) Comparison on the strain-stress curves, strength, Young's modulus, elongation, and toughness between different textile samples. (k) Water vapor permeability of SSLM textiles, commercial fabrics, and casting SEBS film. (l) An intuitive demonstration on the permeability of SSLM E-textiles.

2.2. Electrical and Mechanical Properties

The sheet resistance of the ASEBS textile decreased from 259.69 Ω sq^{-1} to 10.60 Ω sq^{-1}, 3.74 Ω sq^{-1}, and 1.81 Ω sq^{-1} when the sputtering time increased from 5 min to 10 min, 15 min, and 20 min, respectively (Figure S5). Samples sputtered for 15 min were selected for subsequent LM coating considering the decent electrical conductivity and appropriate

depositing time (thickness was 29.3 μm according to the change of fiber diameter). Then, the loading amount of EGaIn was precisely tuned to optimize the electrical and mechanical properties of SSLM E-textiles. As shown in **Figure 2**a, the sheet resistance of SSLM reduced by a magnitude compared to ASEBS when the LM loading was merely 1.0 mg cm^{-2} (124.04 mΩ sq^{-1}), and further decreased to 29.74 mΩ sq^{-1} when the LM loading reached 6 mg cm^{-2}. The electrical resistance change of the E-textiles under strains was also investigated via uniaxial stretching (Figure 2b). Generally, the resistance of the SSLM slowly increased with the gradually increased strains, more LM loading led to the lower increasing slope of the resistance. For the SSLM E-textile with an LM loading of 1 mg cm^{-2}, the resistance increased sharply by 81.8% and 215.1% at strains of 200% and 400%, respectively. Whereas the SSLM-6 (LM loading: 6.0 mg cm^{-2}) microfibers merely increased by 41.5% and 104.5% under the same conditions. Therefore, E-textile with an LM loading amount of 6 mg cm^{-2} was selected for subsequent applications of Joule heater, EMI shielding, and bioelectrode. The conductivity of SSLM textile was further evaluated under 1000 stretching-releasing cycles at 100% strain (Figure 2c), the trifling fluctuation in resistance was ascribed to the stable coating of conducting EGaIn on the highly interconnected and ultra-elastic microfibers. Also owing to the superior stretchability and elasticity, the SSLM E-textile can be easily elongated up to 1000% strain (Figure 2d). When applied as a deformable conductor (Figure 2e), the E-textile can readily light an LED bulb connected to a circuit even under crimpling, stretching (400%), and twisting (720°).

On the other hand, reliable mechanical performance is essential for the durable applications of wearable electronics. Strain-stress curves were measured to evaluate the comprehensive mechanical properties of the ultra-elastic E-textiles. It can be observed in Figure 2f-2j that pristine SEBS microfibers possess the best overall mechanical performance (strength up to 1.89 MPa, Young's modulus reached 150.57 kPa, stretchability as high as 1037%, and toughness over 6.94 MJ m^{-3}). Whereas, post-treatment of Ag-sputtering and LM coating both significantly reduced the mechanical strength, modulus, and toughness of the electronic textiles. Nevertheless, the elongation of the nonwoven showed neglectable changes

after modifications, which was in line with our previous works [49,50], manifesting the unlimited potential of SEBS as a universal stretchable platform for wearable electronics. Moreover, SSLM microfibers with varied LM loading presented very close mechanical performances. For example, the SSLM-6 textile exhibited a strength up to 1.21 MPa, Young's modulus of 64.17 kPa (close to the modulus of human skin) [51], elongation of 1032%, and toughness of 4.80 MJ m^{-3}. Besides, the excellent resilience of SSLM E-textile was also revealed in Figure S6, that only a slight hysteresis could be observed through three consecutive stretch-release cycles in the strain range of 100%-600%.

Apart from desirable mechanical performances, the moisture permeability of skin-attachable electronics plays a vital role in maintaining and regulating the human skin microenvironment. The comparison of water moisture permeability between our E-textiles and commercial textiles is displayed in Figure 2k. Pure SEBS (1965.22 g m^2 day^{-1}) and ASEBS (1980.70 g m^2 day^{-1}) showed comparable vapor permeability as the commercial cotton fabric-1 (2025.91 g m^2 day^{-1}, fabric density: warp×weft = 600×300 threads per 10 cm) and cotton fabric-2 (1936.75 g m^2 day^{-1}, fabric density: warp×weft = 300×300 threads per 10 cm). Conversely, the casted hermetical SEBS film (CSEBS, thickness: ~200 μm) showed poor moisture permeability (37.11 g m^2 day^{-1}), which was widely utilized in stretchable electronic skins and severely suffered from sweat accumulation issues [52]. The pre-stretched SSLM textiles also showed terrific water vapor permeability, for example, the moisture permeability of SSLM-6 reached 1895.49 g m^2 day^{-1}, only a bit lower than that of pure SEBS and ASEBS microfibers. In addition, SSLM E-textile with LM loading of 1-4 mg cm^{-2} showed neglectable vapor permeability degradation, which can perfectly satisfy the daily perspiration needs of human skin. To observe the vapor permeability of the nonwoven intuitively, a piece of SSLM textile (6 mg cm^{-2}) was placed between two glass vials when the bottom one was filled with hot water and the top one was left empty (Figure 2l). Apparently, the water vapor can easily penetrate through the E-textile quickly and condensed on the wall of the top vial in minutes. In another case, the top vial remained dry and empty when the

SSLM textile was replaced by casted SEBS film, proving the superior vapor moisture permeability of the fabricated electronic textiles.

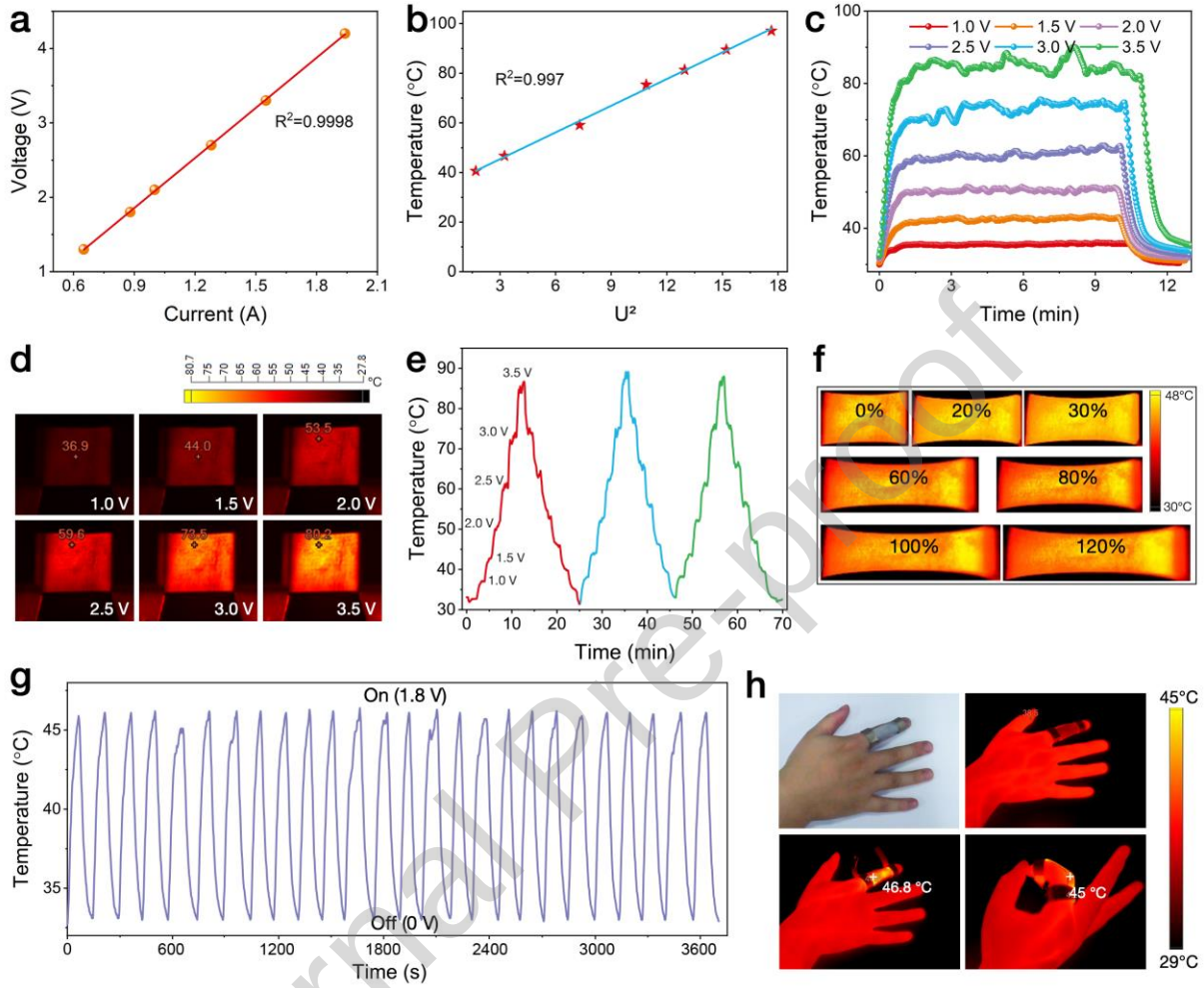

Figure 3. (a) V-I linear curve and (b) T-U^2 curve of SSLM E-textiles. (c) Surface temperature changes and (d) corresponding thermal photos of E-textile with varied input voltages (IR emissivity is 0.95). (e) Repeated saturation temperature change curves during voltage switching. (f) IR photos of SSLM E-textile under 1.8 V during stretching. (g) Electric-to-thermal cycle test curve at 1.8 V. (h) Practical heating application of SSLM E-textiles on a finger under 1.8 V input.

2.3. Joule Heating Performance of SSLM E-Textiles

The highly conductive SSLM E-textiles are expected to possess efficient electro-thermal conversion capabilities owing to the superior conductivity of Gallium-based liquid metal. Herein, the Joule heating properties of SSLM were investigated in detail. **Figure 3**a presents

the linear *I-V* curve of the conducting nonwoven with an LM loading amount of 6.0 mg cm^{-2}, which perfectly follows Ohm's Law (R^2=0.9998). Besides, the U^2-temperature curve also shows high compliance with Joule's Law ($Q=U^2\ R_{resistance}^{-1}\ t$, R^2=0.997) as shown in Figure 3b, proving its high heating maneuverability as electric heaters by tuning the input direct voltage [53]. The electric-thermal conversion performance of the SSLM textile was evaluated with a fixed direct voltage from 1.0 V to 3.5 V for 10 min, and the surface temperature was precisely monitored by an ultrathin patch thermocouple, infrared photos were captured at the same time using Fluke IR camera (Figure 3c and 3d). Evidently, the surface temperature increased synchronously with the stepwise raised voltage, which gradually stabilized at a saturation temperature, manifesting the facile and accurate manipulation of the electric heating performance. It should be noted that the SSLM Joule heater can readily reach its saturation temperature in less than 70 s when the applied voltage is raised, and the temperature also dropped very quickly after cutting off the input voltage. The instability in Figure 3c at 3.5 V is possibly attributed to the unstable contact between LM-encapsulated SEBS fibers in the highly elastic networks, which may enlarge the variation of temperature especially at high voltages.

Besides, the heater also manifested reproducible and recoverable heat output under changing voltages (Figure 3e), demonstrating the rapid and stable electric-thermal conversion performance. Furthermore, the low drive voltage required by SSLM (1.8 V) not only saves energy and ensures human safety (<36 V) [54], but also facilitates the portable and flexible applications of this textile-based Joule heater, which can be readily powered by thin-film or fiber-shaped batteries. Given the super-high elasticity and stable conductivity of the EGaIn-encapsulated E-textiles, the Joule heating performance of SSLM was further assessed under varied strains. Figure 3f depicts that the SSLM E-textile can maintain stable electrical-thermal conversion at a fixed voltage of 1.8V within a large strain range of 0%-120%. To examine the reliability and durability of the SSLM E-textile as a Joule heating device, a cyclic heating/cooling test was carried out under a direct voltage of 1.8 V to verify its long-range stability (Figure 3g). Evidently, there was no noticeable variance in the

temperature curves consisting of 25 continuous cycles, proving the extraordinary performance and dependability of the SSLM heaters. Thus, this permeable and flexible heater can be mounted on the human body as an on-skin Joule heater, which ensures stable thermal generation under continuous and large-scale joint movements such as bending and twisting (Figure 3h).

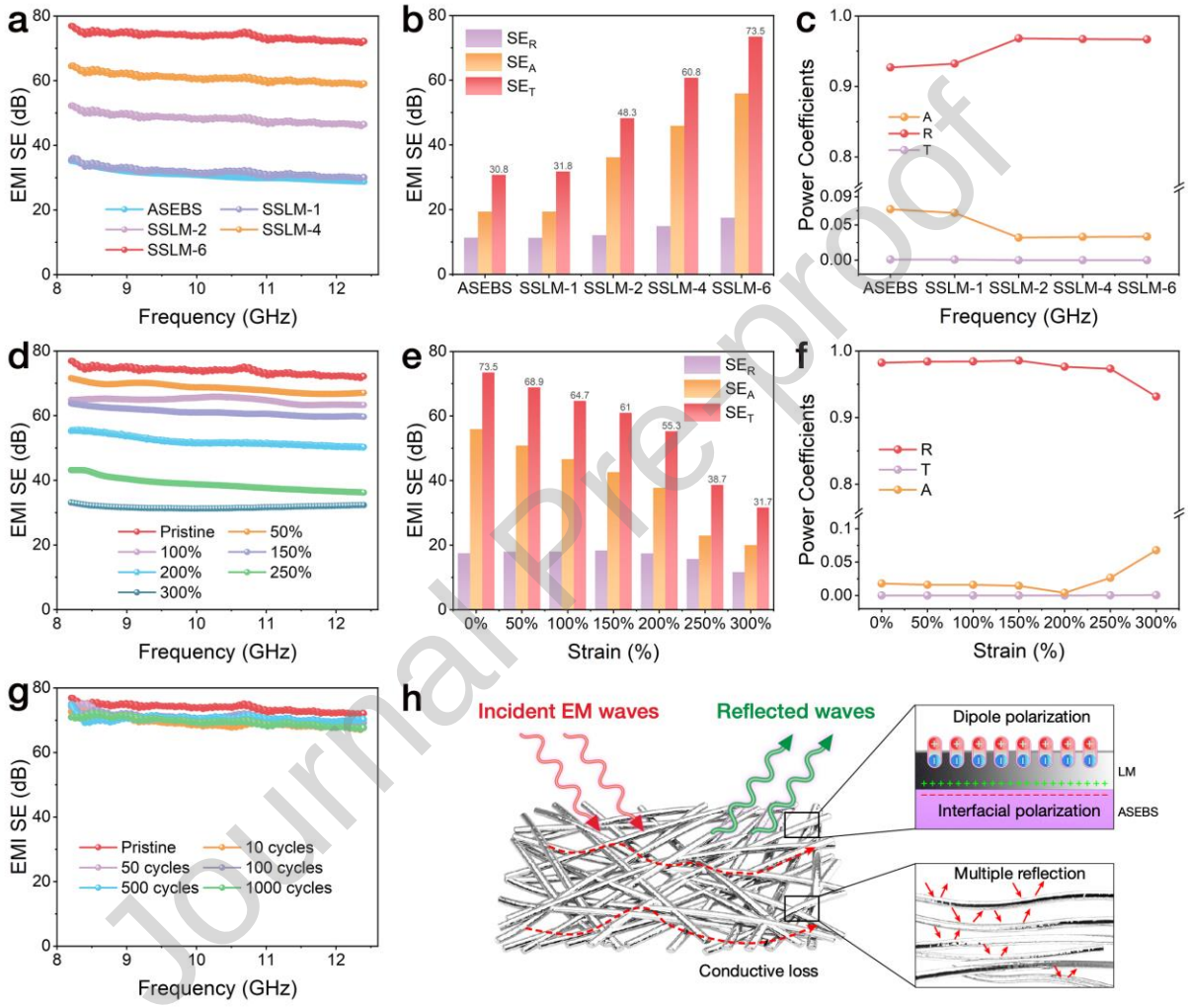

Figure 4. (a) The electromagnetic shielding effectiveness curves of different textiles. (b) The SE_T, SE_A, and SE_R values, and (c) the power coefficients of ASEBS, SSLM textiles. (d) The electromagnetic shielding effectiveness curves, (e) the SE_T, SE_A, and SE_R values, and (f) the power coefficients of SSLM-6 E-textile under various stretching. (g) The electromagnetic shielding performance of SSLM-6 under 100% stretching for 1000 cycles. (h) The electromagnetic shielding mechanism illustration for SSLM E-textiles.

2.4. EMI Shielding Performance of SSLM E-Textiles

With the booming development of a variety of electronic devices including 5G smartphones and micro-computers, the issues of electromagnetic wave pollution have become increasingly prominent which adversely affect human health and surrounding environments [55-59]. Therefore, EMI shielding property is urgently needed by wearable electronics considering their working scenarios. High electrical conductivity is a prerequisite for the design of good EMI shielding materials. The conductivity of the SSLM E-textiles was adjusted by varying the LM loading amount as discussed in the above section. The sheet resistance of SSLM reduced from 3.74 Ω sq^{-1} (ASEBS) to 28.18 mΩ sq^{-1} when the LM loading was 6 mg cm^{-2}. As shown in **Figure 4**a, the EMI shielding performance of SSLM textiles exhibited positive correlations with their electrical conductivity. ASEBS (30.8 dB) and SSLM-1 (31.8 dB) showed very close EMI efficacy, which barely reached the commercial application threshold (>20 dB) [60]. The inefficient EMI SE of ASEBS textile can be ascribed to the ultrathin sputtering layer of Ag nanoparticles, which merely covered the surface of the ASEBS microfibers. Besides, the limited coating of LM in SSLM-1 microfibers was not sufficient to provide a complete network (Figure S7), also resulting in poor EMI performance. Encouragingly, the EMI SE of SSLM-2 textile surged to 48.3 dB when the LM loading amount reached 2 mg cm^{-2}, and continuously increased to 60.8 dB and 73.5 dB as the LM loading rose to 4 mg cm^{-2} and 6 mg cm^{-2}, respectively, proving the outstanding EMI shielding effects delivered by the LM encapsulated nonwoven textiles.

It is known that the parameter absorption efficiency (SE_A) reflects the ability of EMI materials to dissipate the electromagnetic waves that have been transmitted into the materials, whereas the coefficient A (absorption) is the ratio of power attenuated by the EMI materials toward the total incident power. Three power coefficients (absorption (A), reflection (R), and transmission (T)) were obtained from the measured scattering parameters to distinguish the dominant shielding mechanism [61]. The SE_A values of SSLM textiles were much higher than that of reflection efficiency (SE_R) as shown in Figure 4b. For instance, the average total EMI SE (SE_T), SE_A, and SE_R of SSLM-6 microfibers are 73.5, 56.0, and 17.5 dB,

respectively, in which SE_A contributes 76.2% (Figure S8). Moreover, the R values of all SSLM textiles surpassed 90% and increased with the LM amount, revealing that microwave reflection was the main shielding mechanism (Figure 4c) [62]. Figure 4d-4f show the EMI SE performance of the ultra-elastic SSLM E-textile (6.0 mg cm^{-2}) under varied strains of 50-300%. Unstretched SSLM microfibers manifested a SE_T up to 73.5 dB, which still maintained 88% (64.7 dB) of its initial efficiency under 100% strain. Whereas, the SE_T value gradually decreased to 31.7 dB when it was stretched to an ultra-large strain of 300%. As a matter of fact, the homogenously adhered LM coating will deform with the elongated SEBS fibers, which inevitably caused the thinning of the conductive layers and eventually resulted in decreased electrical conductivity. Meanwhile, the microstructure of SSLM E-textile under stretching was observed. As shown in Figure S9, the randomly oriented SSLM fibers became more aligned under strain, leading to the increased electrical contact area between LM-encapsulated fibers, which may compensate the conductivity loss as a result of the thinning of LM coating. However, decreased electrical conductivity was inevitable when large stretching (300%) was imposed. Therefore, the EMI shielding performance of SSLM E-textile degraded as a consequence of large-scale elongation. The power coefficients A, R, and T of stretched SSLM textiles show a similar tendency as the pristine SSLM, disclosing reflection was still the dominant EMI mechanism. Besides, the influence of long-term cyclic stretching/releasing on the EMI shielding stability was investigated on the SSLM E-textile. Surprisingly, SSLM can readily sustain 1000 cycles of stretching at a fixed strain of 100% without sacrificing much EMI SE (Figure 4g and Figure S10), confirming the great stretchability and stability of the conducting networks in SSLM E-textiles. In summary, as-developed SSLM E-textile shows superior EMI SE performance in terms of the highest EMI SE, the widest workable stretchability, and the lowest thickness when compared with recently reported works (Table S1).

Herein, the prominent EMI shielding performance of SSLM nonwoven E-textiles could be ascribed to their outstanding electrical conductivity and interconnected microporosity (as depicted in Figure 4h). When electromagnetic waves strike the surface of the highly

conductive SSLM fibers, numerous EMW energy is reflected on the surface of the material due to impedance mismatching, dissipating the EMW energy as a result of hysteresis loss after converting it into another form of energy (for instance, heat) [63,64]. On the other hand, when EMW gets through the SSLM textile, the interface polarization loss caused by the dipole and charge carriers relaxation between ASEBS and LM assists to absorb incident waves [65]. Meanwhile, current generation during the interaction with LM will cause conductive loss, resulting in an additional decrease in EMW energy. Once the remaining EMW has passed through the surface fibers, it encounters obstacles in the subsequent layer. After that, the inside microfibers act as reflective surfaces and generate multiple internal reflections, resulting in a recurrence of the EMW attenuation phenomenon until the energy is completely absorbed.

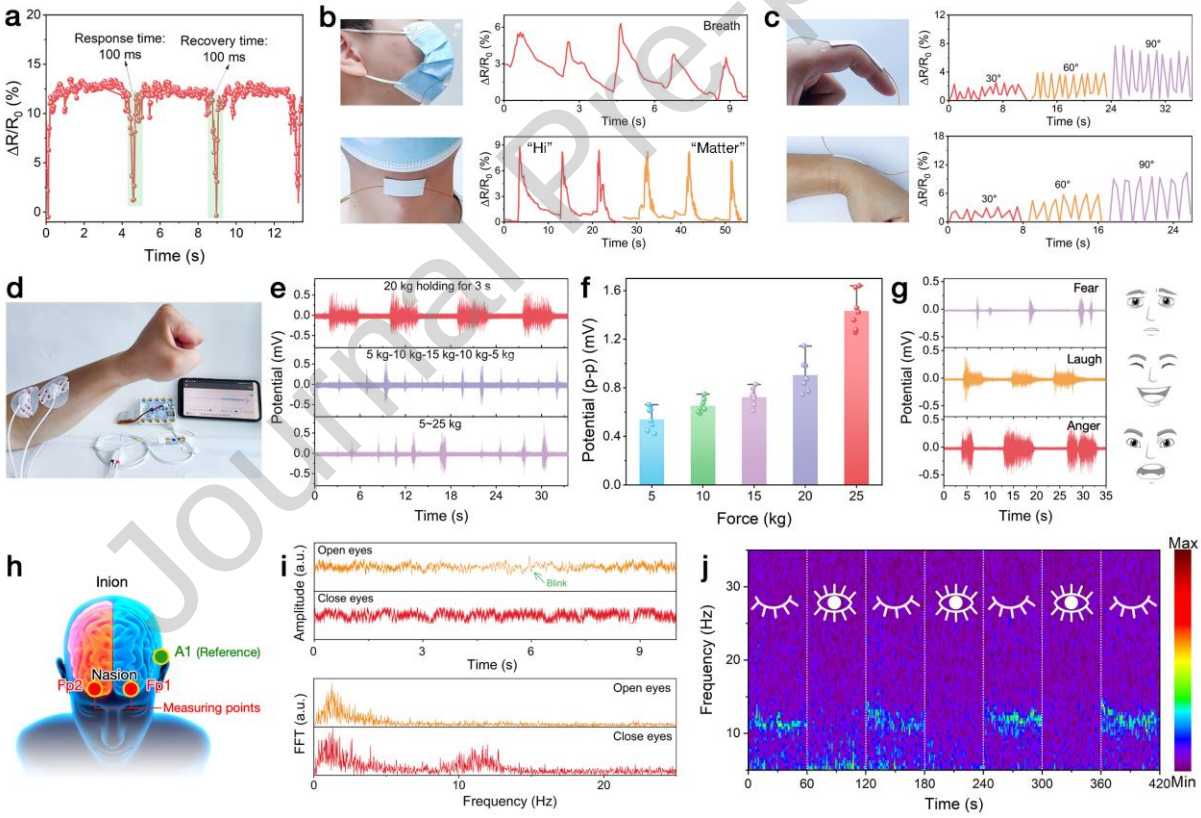

Figure 5. (a) Strain-sensing response and recovery times of SSLM E-textile. (b) Breath and phonation detection, and (c) finger and wrist bending detection using SSLM E-textiles as the strain sensors. (d) Digital photographs of the sEMG detection setup using SSLM as the epidermal bioelectrodes. (e, f) sEMG signals collected from different gripping forces. (g) sEMG signals recorded from different facial expressions (with electrodes attached on face).

(h) Schematic diagram of the EEG measurement position. (i) Recorded EEG signals when the volunteer was engaged in two mental states (closed eyes and open eyes), and the fast Fourier transform (FFT)–processed frequency distributions. (j) Time-frequency spectrograms of the EEG signals recorded during cyclic eye closing/opening, revealing the dynamic activity of the alpha rhythm at about 10 Hz.

2.5. Human Heath Monitoring Applications

The super-high stretchability, low Young's modulus, and excellent conformability empower the nonwoven SSLM E-textile with softness comparable to human skin, in combination with the extraordinary electric conductivity, identifying this material a promising candidate as on-skin bio-electrode to record biophysical and electrophysiological signals including human motions, surface electromyography (sEMG) and electroencephalogram (EEG) [66]. First of all, the strain-sensing behavior of the SSLM textile was measured under tiny tensile strain (1%). It is found that both the response and recovery times of the SSLM electrode were as low as 100 ms (**Figure 5**a), implying the high sensitivity contributed by the crimples on the stretch-activated liquid metal coating. Taking this advantage, the E-textile was then mounted on the skin surface of a tester to assess its capability to monitor human movements. As shown in Figure 5b, the SSLM sensor was able to detect the subtle motions of breath and phonation, as well as larger motions including finger and wrist bending at different angles (Figure 5c). In short, the developed highly conductive SSLM E-textile can be utilized in the accurate and quick detection of complex human motions.

Additionally, sEMG signals were monitored by mounting the E-textile bioelectrodes onto the belly of the extensor digitorum (detection electrodes) and elbow joint (reference electrode) (as depicted in Figure 5d). First of all, in order to evaluate the effects of different gripping forces on the sEMG signals, different extensor contraction actions were recorded. As displayed in Figure 5e, the electrical signals generated by muscle activity can be detected consistently and reproducibly by repeatedly applying 5, 10, 15, 20, and 25 kg of gripping

force to the gripper. It is also important to note that the E-textile bio-electrodes are capable of measuring the steady increase of signal intensity in response to varying forces (Figure 5f), demonstrating the potential of wearable electrodes in the fields of sports management. The SSLM bioelectrodes are able to distinguish different facial movements as a result of their low amplitude signal recognition and high output reliability. As shown in Figure 5g, the bioelectrodes could precisely identify the specific sEMG signals of facial expressions corresponding to the typical moods human experiences in daily life (fear, laughing, and anger), where anger and laughing need more facial muscles to contract, thus resulting in stronger signal intensities. Notably, the signal-to-noise ratio (SNR) measured for the sEMG signal is 23.2 dB.

EEG signals generated by brain activities provide crucial information for various neurological disorders and human emotions. Generally, EEG signals (in the form of waves) can be divided into five frequency bands: δ wave (0 to 4 Hz), θ wave (4 to 8 Hz), α wave (8 to 12 Hz), β wave (12 to 40 Hz), and γ wave (≥40 Hz) [67], corresponding to various mental states. Nevertheless, EEG signals delivered by the human brain are always too weak (μV scale) to be detected, long-time and accurate monitoring of which is extremely challenging. Thanks to the top-notch electrical conductivity, extraordinary skin conformability, and incomparable electrical stability under complex deformations, the SSLM E-textile electrode can be readily used to acquire high-fidelity EEG signals. To evaluate their ability to collect neurophysiological signals, the E-textile electrodes were placed over the left (Fp1) and right (Fp2) side of the forehead as working electrodes, whereas a reference electrode was placed over the left occipital region (A1), according to the international 10-20 system of EEG electrode placement (Figure 5h) [68]. Generally, when a subject is relaxed and with eyes closed, the EEG background typically exhibits the posteriorly dominant α rhythm with a prominent oscillation of 8 to 12 Hz (Figure 5i), in accordance with brain activities such as meditation and mindfulness, which can reduce stress levels. The α rhythm typically attenuates significantly when eye-opening, as can be observed in the EEG signal spectrogram acquired by the SSLM bioelectrodes (Figure 5j), which demonstrates the dynamic activity of

the α rhythm during repeated eye-closing and eye-opening. Lastly, Figure S11 indicates that LM in the E-textile can readily sustain finger rubbing without obvious smearing, guaranteeing the safety mounting and unimpeded accessibility to human bio-signals.

3. Conclusions

In summary, via facile electrospinning, magnetic sputtering, and post liquid metal painting and activation, a highly permeable, ultrastretchable, and conformable electronic textile with super high electromagnetic shielding effectiveness and remarkable Joule heating performance is successfully developed, which could also be applied as advanced epidermal electrodes for long-term personal health monitoring. The densely coated silver nanoparticles greatly facilitate the uniform encapsulation of stretchable EGaIn layer on elastic SEBS microfibers via the fast-alloying process, while pre-stretching activation not only recovers the superior permeability of the nonwoven E-textiles but also endows the E-textiles with excellent stability and conductivity even under large strains up to 1000%. Thus, an EMI shielding effectiveness of 75.3 dB at frequencies of 8.2-12.8 GHz can be readily achieved, which even maintains 31.7 dB at 300% elongation. When being employed as wearable and stretchable Joule heaters, the nonwoven E-textile can assure stable thermal output under 120% deformation. What is more, skin-attachable bioelectrodes assembled using the developed E-textiles even manifest prominent biophysical (breath, phonation, and joint bending) and bioelectrical signals (sEMG and EEG) monitoring performance. This research offers a promising alternative to produce multi-functional on-skin bioelectronics for safe and comfortable personal health management.

4. Experimental

4.1. Materials

Elastomer styrene-ethylene-butylene-styrene (SEBS, commercial purity) was supplied by Kraton Corp. Silver sputtering targets (purity: 99.99%) were purchased from Fuzhou Invention photoelectrical Technology. Gallium–Indium eutectic (EGaIn, Ga 75.5%/In 24.5%,

melting point: 15.6 °C, 99.99%) was obtained from Dongguan Huatai Metal Material Technology Co., Ltd. All the laboratory solvents (AR) were purchased from Sinopharm Chemical Reagent Corp.

4.2. Fabrication of highly stretchable SEBS microfibers

SEBS was dissolved in chloroform/toluene (mass ratio: 9/1) to prepare the SEBS solution in a mass concentration of 15 wt.%, a few drops of ionic liquid were then added into the solution to increase the electric conductance. The electrospun microfibers were received with a steel grid to assure the optimized permeability on both sides of the nonwoven (detailed electrospinning parameters can be found in our previously works[49,50]). The thickness of the electrospun microfiber films was about 200 μm. As-spun SEBS nonwoven textiles were annealed at 105 °C for 60 min before peeling off from the steel grid, followed by washing with ethanol and drying at ambient temperature.

4.3. Fabrication of permeable liquid metal E-textiles

Silver sputtering was firstly conducted through a multifunctional high-vacuum magnetron sputtering equipment (JZCK-420B). Briefly, the sputtering process was initiated after the chamber pressure stabilized below 8.8×10^{-4} Pa, the Argon flow was kept at 25 mL min^{-1} and the sputtering power maintain at 40 W. Obtained nano-silver deposited SEBS textiles were termed as ASEBS-5, ASEBS-10, ASEBS-15, and ASEBS-20, respectively, according to different sputtering times (5 min, 10 min, 15 min, and 20 min). For the coating of liquid metal, the ASEBS textiles were first cut into rectangular pieces with the dimension of 4 × 5 cm^2, then different amount of gallium-indium eutectic was weighed according to required coating amount. After that, EGaIn was transferred and evenly coated onto the ASEBS nonwoven matrixes via a simple painting technique using a silicone brush, followed by repeated monolithic stretching to activate the conductive textiles (denoted as SSLM). The amount of LM can be controlled simply by changing the weight during brushing.

4.4. Materials Characterizations

SEM images were taken with a Hitachi S-4800 FE-SEM. Optical images were captured by a Keyence VHX-1000C Ultra Depth Microscope. 3D morphology was recorded using a Keyence VK-X150 Laser Microscope. Contact angles were measured via the Dataphysics OCA15EC contact angle system. XRD patterns were recorded via a Bruker AXS D2 PHASER X-ray diffractometer. The sheet resistance was measured through a ST2263 double-testing digital four-probe tester under a four-point configuration. Water moisture permeability was determined on a W3/060 Water Vapor Transmission Rate Test System (temperature: 38 °C, humidity: 80 RH%). Mechanical properties were measured via a Sun Technology universal UTM2203 tensile testing machine. Electromechanical properties were studied utilizing a Keysight 34465A digital meter coupled with a Mark-10 ESM303 tensile tester.

The E-textiles were cut into circular shapes to assemble the on-skin electrode patches for biosignal measurement. As-collected signals were transferred to a cell phone or computer via the Bluetooth module. EEG signals were converted through the following equation (valid EEG sensor range: -39.49 μV to +39.49 μV):

$$EEG\ (\mu V) = \frac{\left(\frac{ADC}{2^n} - \frac{1}{2}\right) \times VCC \times 10^6}{G_{EEG}} \qquad (1)$$

where *EEG (μV)* is the EEG signal in microvolt (μV), *VCC* is the operating voltage (3.3 V), G_{EEG} is the sensor gain (41782), *ADC* is the collected digital value from the corresponding channel, *n* is the bit number of the channel (10 bits in this work).

In order to acquire high-quality EEG signals, the signal collection was carried out in a quiet room, and the volunteer was required to wear a noise-canceling headphone to block potential noise. The acquired time-domain signals were then transformed into frequency spectra to analyze the brain activity rhythm via discrete Fourier transform (DFT, equation 2-3) and periodogram method (equation 4). Whereas the EEG spectrogram was conducted through a short-time Fourier transform (STFT, Welch window).

$$f = \frac{kF_S}{N} \ \ (k = 0, 1, \ldots, N-1) \qquad (2)$$

$$F[k] = \sum_{n=0}^{N-1} x[n] e^{-\frac{j2\pi kn}{N}} \quad (3)$$

$$P(f) = \frac{1}{NF_S} \left[\sum_{n=1}^{N} x[n] e^{-\frac{j2\pi fn}{F_S}} \right]^2 \quad (4)$$

Where N is the total sampling points, f is the frequency, $x[n]$ is the timing signal, Fs is the sampling frequency.

Similarly, the recorded sEMG signals were also processed through equation 5 (valid sEMG sensor range: -1.64 mV to +1.64 mV):

$$sEMG\ (mV) = \frac{\left(\frac{ADC}{2^n} - \frac{1}{2}\right) \times VCC \times 10^3}{G_{sEMG}} \quad (5)$$

where *sEMG (mV)* is the sEMG signal in millivolt (mV), *VCC* is the operating voltage (3.3 V), G_{sEMG} is the sensor gain (1009), *ADC* is the collected digital value from the corresponding channel, *n* is sampling resolution (10 bits).

The signal-to-noise ratio (SNR) of the E-textile electrode is calculated according to the following equation (6):

$$SNR\ (dB) = 20 \times \log_{10} \frac{\sqrt{\sum_{k=1}^{N} V_{signal(k)}^2}}{\sqrt{\sum_{k=1}^{N} V_{noise(k)}^2}} \quad (6)$$

where N is the number of samples, $V_{signal(k)}$ and $V_{noise(k)}$ are the voltage values of the signal and noise, respectively.

The EMI performance of the highly conductive E-textiles was measured via a Keysight N5234B PNA-L Network Analyzer using a 2-port network analyzer at a frequency range of 8.2 GHz-12.4 GHz. The scattering parameters of the reflection coefficient data S_{11} and the transmission data S_{21} were measured to calculate the power coefficients of reflection (R), transmission (T), and absorption (A).

$$R = [S_{11}]^2 \text{ and } T = [S_{21}]^2 \quad (7)$$

$$A = 1 - (T + R) \quad (8)$$

The calculation of total EMI SE (SE_T), reflection efficiency (SE_R), absorption efficiency (SE_A), and multiple reflection efficiency (SE_M) is as follows:

$$SE_T = 10log\frac{1}{T} \quad (9)$$

$$SE_R = 10log\left(\frac{1-R}{T}\right) \quad (10)$$

$$SE_A = 10log\left(\frac{1-R}{T}\right) \quad (11)$$

$$SE_T = SE_R + SE_A + SE_M \quad (12)$$

Where SE_M could be negligible when SE_{total} > 15 dB.

Acknowledgements

This work is financially supported by the National Natural Science Foundation of China (21875033, 52161135302), the Research Foundation Flanders (G0F2322N), the China Postdoctoral Science Foundation (2022M711355), the Natural Science Foundation of Jiangsu Province (BK20221540), the Shanghai Scientific and Technological Innovation Project (18JC1410600), the Program of the Shanghai Academic Research Leader (17XD1400100), the State Key Laboratory for Modification of Chemical Fibers and Polymer Materials, Donghua University, and the Postgraduate Research & Practice Innovation Program of Jiangsu Province (KYCX22_2317). We also appreciate greatly the instrumental characterization services provided by Central Laboratory, School of Chemical and Material Engineering, Jiangnan University.

Conflict of Interest

The authors declare no conflict of interest.

References

[1] H. Shim, S. Jang, A. Thukral, S. Jeong, H. Jo, B. Kan, S. Patel, G. Wei, W. Lan, H.-J. Kim, C. Yu, Artificial neuromorphic cognitive skins based on distributed biaxially stretchable elastomeric synaptic transistors, Proc. Natl. Acad. Sci. 119 (2022) e2204852119, https://doi.org/10.1073/pnas.2204852119.

[2] Y. Dai, H. Hu, M. Wang, J. Xu, S. Wang, Stretchable transistors and functional circuits for human-integrated electronics, Nat. Electron. 4 (2021) 17-29, https://doi.org/10.1038/s41928-020-00513-5.

[3] Z. Ma, X. Xiang, L. Shao, Y. Zhang, J. Gu, Multifunctional Wearable Silver Nanowire Decorated Leather Nanocomposites for Joule Heating, Electromagnetic Interference Shielding and Piezoresistive Sensing, Angew. Chem., Int. Ed. 61 (2022) e202200705, https://doi.org/10.1002/anie.202200705.

[4] X. Yu, Z. Xie, Y. Yu, J. Lee, A. Vazquez-Guardado, H. Luan, J. Ruban, X. Ning, A. Akhtar, D. Li, B. Ji, Y. Liu, R. Sun, J. Cao, Q. Huo, Y. Zhong, C. Lee, S. Kim, P. Gutruf, C. Zhang, Y. Xue, Q. Guo, A. Chempakasseril, P. Tian, W. Lu, J. Jeong, Y. Yu, J. Cornman, C. Tan, B. Kim, K. Lee, X. Feng, Y. Huang, J.A. Rogers, Skin-integrated wireless haptic interfaces for virtual and augmented reality, Nature 575 (2019) 473-479, https://doi.org/10.1038/s41586-019-1687-0.

[5] X. Liu, The more and less of electronic-skin sensors, Science 370 (2020) 910-911, https://doi.org/10.1126/science.abe7366.

[6] X. Shi, Y. Zuo, P. Zhai, J. Shen, Y. Yang, Z. Gao, M. Liao, J. Wu, J. Wang, X. Xu, Q. Tong, B. Zhang, B. Wang, X. Sun, L. Zhang, Q. Pei, D. Jin, P. Chen, H. Peng, Large-area display textiles integrated with functional systems, Nature 591 (2021) 240-245, https://doi.org/10.1038/s41586-021-03295-8.

[7] Y. Yu, J. Li, S.A. Solomon, J. Min, J. Tu, W. Guo, C. Xu, Y. Song, W. Gao, All-printed soft human-machine interface for robotic physicochemical sensing, Sci. Robot. 7 (2022) eabn0495, https://doi.org/10.1126/scirobotics.abn0495.

[8] Y. Wang, D. Yang, M.M. Hessien, K. Du, M.M. Ibrahim, Y. Su, G.A.M. Mersal, R. Ma, S.M. El-Bahy, M. Huang, Q. Yuan, B. Cui, D. Hu, Flexible barium titanate@polydopamine/polyvinylidene fluoride/polymethyl methacrylate nanocomposite films with high performance energy storage, Adv. Compos. Hybrid Mater. 5 (2022) 2106-2115, https://doi.org/10.1007/s42114-022-00552-w.

[9] S. Gao, X. Zhao, Q. Fu, T. Zhang, J. Zhu, F. Hou, J. Ni, C. Zhu, T. Li, Y. Wang, V. Murugadoss, G.A.M. Mersal, M.M. Ibrahim, Z.M. El-Bahy, M. Huang, Z. Guo, Highly transmitted silver nanowires-SWCNTs conductive flexible film by nested density structure

and aluminum-doped zinc oxide capping layer for flexible amorphous silicon solar cells, J. Mater. Sci. Technol. 126 (2022) 152-160, https://doi.org/10.1016/j.jmst.2022.03.012.

[10] L. Li, Y. Zhang, H. Lu, Y. Wang, J. Xu, J. Zhu, C. Zhang, T. Liu, Cryopolymerization enables anisotropic polyaniline hybrid hydrogels with superelasticity and highly deformation-tolerant electrochemical energy storage, Nat. Commun. 11 (2020) 62, https://doi.org/10.1038/s41467-019-13959-9.

[11] K. Chang, L. Li, C. Zhang, P. Ma, W. Dong, Y. Huang, T. Liu, Compressible and robust PANI sponge anchored with erected MXene flakes for human motion detection, Composites, Part A 151 (2021) 106671, https://doi.org/10.1016/j.compositesa.2021.106671.

[12] L. Pu, H. Ma, J. Dong, C. Zhang, F. Lai, G. He, P. Ma, W. Dong, Y. Huang, T. Liu, Xylem-Inspired Polyimide/MXene Aerogels with Radial Lamellar Architectures for Highly Sensitive Strain Detection and Efficient Solar Steam Generation, Nano Lett. 22 (2022) 4560–4568, https://doi.org/10.1021/acs.nanolett.2c01486.

[13] Z. Ma, Q. Huang, Q. Xu, Q. Zhuang, X. Zhao, Y. Yang, H. Qiu, Z. Yang, C. Wang, Y. Chai, Z. Zheng, Permeable superelastic liquid-metal fibre mat enables biocompatible and monolithic stretchable electronics, Nat. Mater. 20 (2021) 859-868, https://doi.org/10.1038/s41563-020-00902-3.

[14] H. Guo, Y. Li, Y. Ji, Y. Chen, K. Liu, B. Shen, S. He, G. Duan, J. Han, S. Jiang, Highly flexible carbon nanotubes/aramid nanofibers composite papers with ordered and layered structures for efficient electromagnetic interference shielding, Compos. Commun. 27 (2021) 100879, https://doi.org/10.1016/j.coco.2021.100879.

[15] D.O. Carpenter, Human disease resulting from exposure to electromagnetic fields, Rev. Environ. Health 28 (2013) 159-172, https://doi.org/10.1515/reveh-2013-0016.

[16] M.M. Salman, H.I. Kemp, M.R. Cauldwell, D.P. Dob, R. Sutton, Anaesthetic management of pregnant patients with cardiac implantable electronic devices: case reports and review, Int. J. Obstet. Anesth 33 (2018) 57-66, https://doi.org/10.1016/j.ijoa.2017.07.011.

[17] R. Dilli, R. Ch, r.M. L , D. Jordhana, Ultra-Massive Multiple Input Multiple Output Technologies for 6G Wireless Networks, Eng. Sci. 16 (2021) 308-318, https://doi.org/10.30919/es8d571.

[18] F. Luo, D. Liu, T. Cao, H. Cheng, J. Kuang, Y. Deng, W. Xie, Study on broadband microwave absorbing performance of gradient porous structure, Adv. Compos. Hybrid Mater. 4 (2021) 591-601, https://doi.org/10.1007/s42114-021-00275-4.

[19] Y. Zhang, J. Kong, J. Gu, New generation electromagnetic materials: harvesting instead of dissipation solo, Sci. Bull. 67 (2022) 1413-1415, https://doi.org/10.1016/j.scib.2022.06.017.

[20] F. Shahzad, M. Alhabeb, C.B. Hatter, B. Anasori, S. Man Hong, C.M. Koo, Y. Gogotsi, Electromagnetic interference shielding with 2D transition metal carbides (MXenes), Science 353 (2016) 1137-1140, https://doi.org/10.1126/science.aag2421.

[21] G. Yang, K. Zhu, W. Guo, D. Wu, X. Quan, X. Huang, S. Liu, Y. Li, H. Fang, Y. Qiu, Q. Zheng, M. Zhu, J. Huang, Z. Zeng, Z. Yin, H. Wu, Adhesive and Hydrophobic Bilayer Hydrogel Enabled On-Skin Biosensors for High-Fidelity Classification of Human Emotion, Adv. Funct. Mater. 32 (2022) 2200457, https://doi.org/10.1002/adfm.202200457.

[22] Y. Zhang, Z. Ma, K. Ruan, J. Gu, Multifunctional Ti3C2Tx-(Fe3O4/polyimide) composite films with Janus structure for outstanding electromagnetic interference shielding and superior visual thermal management, Nano Res. 15 (2022) 5601-5609, https://doi.org/10.1007/s12274-022-4358-7.

[23] P. Song, B. Liu, C. Liang, K. Ruan, H. Qiu, Z. Ma, Y. Guo, J. Gu, Lightweight, Flexible Cellulose-Derived Carbon Aerogel@Reduced Graphene Oxide/PDMS Composites with Outstanding EMI Shielding Performances and Excellent Thermal Conductivities, Nano-Micro Lett. 13 (2021) 91, https://doi.org/10.1007/s40820-021-00624-4.

[24] C. Liu, W. Wu, Y. Wang, Z. Wang, Q. Chen, Silver-coated thermoplastic polyurethane hybrid granules for dual-functional elastomer composites with exceptional thermal conductive and electromagnetic interference shielding performances, Compos. Commun. 25 (2021) 100719, https://doi.org/10.1016/j.coco.2021.100719.

[25] Z. Ye, Y. Ling, M. Yang, Y. Xu, L. Zhu, Z. Yan, P.-Y. Chen, A Breathable, Reusable, and Zero-Power Smart Face Mask for Wireless Cough and Mask-Wearing Monitoring, ACS Nano 16 (2022) 5874–5884., https://doi.org/10.1021/acsnano.1c11041.

[26] S. Fallah, H.R. Mamaghani, R. Yegani, N. Hajinajaf, B. Pourabbas, Use of graphene substrates for wastewater treatment of textile industries, Adv. Compos. Hybrid Mater. 3 (2020) 187-193, https://doi.org/10.1007/s42114-020-00146-4.

[27] W. Zhang, M. Jiang, S. Yang, Y. Hu, B. Mu, Z. Tie, Z. Jin, In-situ grown CuOx nanowire forest on copper foam: A 3D hierarchical and freestanding electrocatalyst with enhanced carbonaceous product selectivity in CO2 reduction, Nano Res. Energy 1 (2022) e9120033, https://doi.org/10.26599/NRE.2022.9120033.

[28] K. Pan, Y. Shi, J. Qiu, Deformation regulated flexible carbon foam matrix intrinsic metamaterials, Compos. Commun. 27 (2021) 100820, https://doi.org/10.1016/j.coco.2021.100820.

[29] S. Li, X. Tang, X. Zhao, S. Lu, J. Luo, Z. Chai, T. Ma, Q. Lan, P. Ma, W. Dong, Z. Wang, T. Liu, Hierarchical graphene@MXene composite foam modified with flower-shaped FeS for efficient and broadband electromagnetic absorption, J. Mater. Sci. Technol. 133 (2023) 238-248, https://doi.org/10.1016/j.jmst.2022.06.018.

[30] Z. Du, K. Chen, Y. Zhang, Y. Wang, P. He, H.-Y. Mi, Y. Wang, C. Liu, C. Shen, Engineering multilayered MXene/electrospun poly(lactic acid) membrane with increscent electromagnetic interference (EMI) shielding for integrated Joule heating and energy generating, Compos. Commun. 26 (2021) 100770, https://doi.org/10.1016/j.coco.2021.100770.

[31] L. Pu, Y. Liu, L. Li, C. Zhang, P. Ma, W. Dong, Y. Huang, T. Liu, Polyimide Nanofiber-Reinforced Ti3C2Tx Aerogel with “Lamella-Pillar” Microporosity for High-Performance Piezoresistive Strain Sensing and Electromagnetic Wave Absorption, ACS Appl. Mater. Interfaces 13 (2021) 47134-47146, https://doi.org/10.1021/acsami.1c13863.

[32] N. Wu, B. Zhao, X. Chen, C. Hou, M. Huang, A. Alhadhrami, G.A.M. Mersal, M.M. Ibrahim, J. Tian, Dielectric properties and electromagnetic simulation of molybdenum

disulfide and ferric oxide-modified Ti3C2TX MXene hetero-structure for potential microwave absorption, Adv. Compos. Hybrid Mater. 5 (2022) 1548-1556, https://doi.org/10.1007/s42114-022-00490-7.

[33] Y. Bai, L. Sun, Q. Yu, Y. Lei, B. Liu, Biomolecule capturing and sensing on 2D transition metal dichalcogenide canvas, Nano Res. Energy (2022), https://doi.org/10.26599/NRE.2023.9120043.

[34] M.D. Dickey, Stretchable and Soft Electronics using Liquid Metals, Adv. Mater. 29 (2017) 1606425, https://doi.org/10.1002/adma.201606425.

[35] J. Dong, Y. Peng, X. Nie, L. Li, C. Zhang, F. Lai, G. He, P. Ma, Q. Wei, Y. Huang, T. Liu, Hierarchically Designed Super-Elastic Metafabric for Thermal-Wet Comfortable and Antibacterial Epidermal Electrode, Adv. Funct. Mater. (2022) 2209762, https://doi.org/10.1002/adfm.202209762.

[36] K.Y. Kwon, S. Cheeseman, A. Frias-De-Diego, H. Hong, J. Yang, W. Jung, H. Yin, B.J. Murdoch, F. Scholle, N. Crook, E. Crisci, M.D. Dickey, V.K. Truong, T.-i. Kim, A Liquid Metal Mediated Metallic Coating for Antimicrobial and Antiviral Fabrics, Adv. Mater. 33 (2021) 2104298, https://doi.org/10.1002/adma.202104298.

[37] X. Ma, M. Zhang, J. Zhang, S. Wang, S. Cao, Y. Li, G. Hu, D. Kong, Highly Permeable and Ultrastretchable Liquid Metal Micromesh for Skin-Attachable Electronics, ACS Mater. Lett. 4 (2022) 634-641, https://doi.org/10.1021/acsmaterialslett.1c00763.

[38] S.-Y. Tang, C. Tabor, K. Kalantar-Zadeh, M.D. Dickey, Gallium Liquid Metal: The Devil's Elixir, Annu. Rev. Mater. Res. 51 (2021) 381-408, https://doi.org/10.1146/annurev-matsci-080819-125403.

[39] P. Wu, J. Fu, Y. Xu, Y. He, Liquid Metal Microgels for Three-Dimensional Printing of Smart Electronic Clothes, ACS Appl. Mater. Interfaces 14 (2022) 13458-13467, https://doi.org/10.1021/acsami.1c22975.

[40] X. Li, M. Li, L. Zong, X. Wu, J. You, P. Du, C. Li, Liquid Metal Droplets Wrapped with Polysaccharide Microgel as Biocompatible Aqueous Ink for Flexible Conductive Devices, Adv. Funct. Mater. 28 (2018) 1804197, https://doi.org/10.1002/adfm.201804197.

[41] L. Tang, L. Mou, W. Zhang, X. Jiang, Large-Scale Fabrication of Highly Elastic Conductors on a Broad Range of Surfaces, ACS Appl. Mater. Interfaces 11 (2019) 7138-7147, https://doi.org/10.1021/acsami.8b20460.

[42] Q. Zhuang, Z. Ma, Y. Gao, Y. Zhang, S. Wang, X. Lu, H. Hu, C. Cheung, Q. Huang, Z. Zheng, Liquid–Metal-Superlyophilic and Conductivity–Strain-Enhancing Scaffold for Permeable Superelastic Conductors, Adv. Funct. Mater. 31 (2021) 2105587, https://doi.org/10.1002/adfm.202105587.

[43] J.-H. Kim, S. Kim, H. Kim, S. Wooh, J. Cho, M.D. Dickey, J.-H. So, H.-J. Koo, Imbibition-induced selective wetting of liquid metal, Nat. Commun. 13 (2022) 4763, https://doi.org/10.1038/s41467-022-32259-3.

[44] X. Sun, J. Sun, T. Li, S. Zheng, C. Wang, W. Tan, J. Zhang, C. Liu, T. Ma, Z. Qi, C. Liu, N. Xue, Flexible Tactile Electronic Skin Sensor with 3D Force Detection Based on Porous CNTs/PDMS Nanocomposites, Nano-Micro Lett. 11 (2019) 57, https://doi.org/10.1007/s40820-019-0288-7.

[45] C. Shi, Z. Zou, Z. Lei, P. Zhu, W. Zhang, J. Xiao, Heterogeneous integration of rigid, soft, and liquid materials for self-healable, recyclable, and reconfigurable wearable electronics, Sci. Adv. 6 (2020) eabd0202, https://doi.org/10.1126/sciadv.abd0202.

[46] A. Hajalilou, A.F. Silva, P.A. Lopes, E. Parvini, C. Majidi, M. Tavakoli, Biphasic Liquid Metal Composites for Sinter-Free Printed Stretchable Electronics, Adv. Mater. Interfaces 9 (2022) 2101913, https://doi.org/10.1002/admi.202101913.

[47] J. Cao, F. Liang, H. Li, X. Li, Y. Fan, C. Hu, J. Yu, J. Xu, Y. Yin, F. Li, D. Xu, H. Feng, H. Yang, Y. Liu, X. Chen, G. Zhu, R.-W. Li, Ultra-robust stretchable electrode for e-skin: In situ assembly using a nanofiber scaffold and liquid metal to mimic water-to-net interaction, InfoMat 4 (2022) e12302, https://doi.org/10.1002/inf2.12302.

[48] H. Wang, S. Chen, X. Zhu, B. Yuan, X. Sun, J. Zhang, X. Yang, Y. Wei, J. Liu, Phase transition science and engineering of gallium-based liquid metal, Matter 5 (2022) 2054-2085, https://doi.org/10.1016/j.matt.2022.05.031.

[49] J. Dong, D. Wang, Y. Peng, C. Zhang, F. Lai, G. He, P. Ma, W. Dong, Y. Huang, I.P. Parkin, T. Liu, Ultra-Stretchable and Superhydrophobic Textile-Based Bioelectrodes for Robust Self-Cleaning and Personal Health Monitoring, Nano Energy 97 (2022) 107160, https://doi.org/10.1016/j.nanoen.2022.107160.

[50] J. Dong, L. Li, C. Zhang, P. Ma, W. Dong, Y. Huang, T. Liu, Ultra-highly stretchable and anisotropic SEBS/F127 fiber films equipped with an adaptive deformable carbon nanotube layer for dual-mode strain sensing, J. Mater. Chem. A 9 (2021) 18294-18305, https://doi.org/10.1039/D1TA04563F.

[51] P. Tan, H. Wang, F. Xiao, X. Lu, W. Shang, X. Deng, H. Song, Z. Xu, J. Cao, T. Gan, B. Wang, X. Zhou, Solution-processable, soft, self-adhesive, and conductive polymer composites for soft electronics, Nat. Commun. 13 (2022) 358, https://doi.org/10.1038/s41467-022-28027-y.

[52] N. Jiang, H. Li, D. Hu, Y. Xu, Y. Hu, Y. Zhu, X. Han, G. Zhao, J. Chen, X. Chang, M. Xi, Q. Yuan, Stretchable strain and temperature sensor based on fibrous polyurethane film saturated with ionic liquid, Compos. Commun. 27 (2021) 100845, https://doi.org/10.1016/j.coco.2021.100845.

[53] Y. Shi, Z. Xiang, L. Cai, F. Pan, Y. Dong, X. Zhu, J. Cheng, H. Jiang, W. Lu, Multi-interface Assembled N-Doped MXene/HCFG/AgNW Films for Wearable Electromagnetic Shielding Devices with Multimodal Energy Conversion and Healthcare Monitoring Performances, ACS Nano 16 (2022) 7816–7833., https://doi.org/10.1021/acsnano.2c00448.

[54] S. Gong, X. Sheng, X. Li, M. Sheng, H. Wu, X. Lu, J. Qu, A Multifunctional Flexible Composite Film with Excellent Multi-Source Driven Thermal Management, Electromagnetic Interference Shielding, and Fire Safety Performance, Inspired by a “Brick–Mortar” Sandwich Structure, Adv. Funct. Mater. 32 (2022) 2200570, https://doi.org/10.1002/adfm.202200570.

[55] Y. Zhang, S. Li, X. Tang, W. Fan, Q. Lan, L. Li, P. Ma, W. Dong, Z. Wang, T. Liu, Ultralight and ordered lamellar polyimide-based graphene foams with efficient broadband

electromagnetic absorption, J. Mater. Sci. Technol. 102 (2022) 97-104, https://doi.org/10.1016/j.jmst.2021.07.011.

[56] L. Pu, S. Li, Y. Zhang, H. Zhu, W. Fan, P. Ma, W. Dong, Z. Wang, T. Liu, Polyimide-based graphene composite foams with hierarchical impedance gradient for efficient electromagnetic absorption, J. Mater. Chem. C 9 (2021) 2086-2094, https://doi.org/10.1039/D0TC04951D.

[57] S. Li, X. Tang, Y. Zhang, Q. Lan, Z. Hu, L. Li, N. Zhang, P. Ma, W. Dong, W. Tjiu, Z. Wang, T. Liu, Corrosion-Resistant Graphene-Based Magnetic Composite Foams for Efficient Electromagnetic Absorption, ACS Appl. Mater. Interfaces 14 (2022) 8297-8310, https://doi.org/10.1021/acsami.1c23439.

[58] X. Tang, J. Luo, Z. Hu, S. Lu, X. Liu, S. Li, X. Zhao, Z. Zhang, Q. Lan, P. Ma, Z. Wang, T. Liu, Ultrathin, flexible and oxidation-resistant MXene/Graphene porous films for efficient electromagnetic interference shielding, Nano Res. (2022), https://doi.org/10.1007/s12274-022-4841-1.

[59] L. Wang, Z. Ma, H. Qiu, Y. Zhang, Z. Yu, J. Gu, Significantly Enhanced Electromagnetic Interference Shielding Performances of Epoxy Nanocomposites with Long-Range Aligned Lamellar Structures, Nano-Micro Lett. 14 (2022) 224, https://doi.org/10.1007/s40820-022-00949-8.

[60] M. Wang, X.-H. Tang, J.-H. Cai, H. Wu, J.-B. Shen, S.-Y. Guo, Construction, mechanism and prospective of conductive polymer composites with multiple interfaces for electromagnetic interference shielding: A review, Carbon 177 (2021) 377-402, https://doi.org/10.1016/j.carbon.2021.02.047.

[61] Y. Xu, Z. Lin, K. Rajavel, T. Zhao, P. Zhu, Y. Hu, R. Sun, C.-P. Wong, Tailorable, Lightweight and Superelastic Liquid Metal Monoliths for Multifunctional Electromagnetic Interference Shielding, Nano-Micro Lett. 14 (2021) 29, https://doi.org/10.1007/s40820-021-00766-5.

[62] S.-Q. Yi, H. Sun, Y.-F. Jin, K.-K. Zou, J. Li, L.-C. Jia, D.-X. Yan, Z.-M. Li, CNT-assisted design of stable liquid metal droplets for flexible multifunctional composites, Composites, Part B 239 (2022) 109961, https://doi.org/10.1016/j.compositesb.2022.109961.

[63] Q.-W. Wang, H.-B. Zhang, J. Liu, S. Zhao, X. Xie, L. Liu, R. Yang, N. Koratkar, Z.-Z. Yu, Multifunctional and Water-Resistant MXene-Decorated Polyester Textiles with Outstanding Electromagnetic Interference Shielding and Joule Heating Performances, Adv. Funct. Mater. 29 (2019) 1806819, https://doi.org/10.1002/adfm.201806819.

[64] W. Chen, L.-X. Liu, H.-B. Zhang, Z.-Z. Yu, Flexible, Transparent, and Conductive Ti3C2Tx MXene–Silver Nanowire Films with Smart Acoustic Sensitivity for High-Performance Electromagnetic Interference Shielding, ACS Nano 14 (2020) 16643-16653, https://doi.org/10.1021/acsnano.0c01635.

[65] R. Zhu, Z. Li, G. Deng, Y. Yu, J. Shui, R. Yu, C. Pan, X. Liu, Anisotropic magnetic liquid metal film for wearable wireless electromagnetic sensing and smart electromagnetic interference shielding, Nano Energy 92 (2022) 106700, https://doi.org/10.1016/j.nanoen.2021.106700.

[66] H. Hu, Y. Ma, J. Yue, F. Zhang, Porous GNP/PDMS composites with significantly reduced percolation threshold of conductive filler for stretchable strain sensors, Compos. Commun. 29 (2022) 101033, https://doi.org/10.1016/j.coco.2021.101033.

[67] Y. Xu, W. Guo, S. Zhou, H. Yi, G. Yang, S. Mei, K. Zhu, H. Wu, Z. Li, Bioinspired Perspiration-Wicking Electronic Skins for Comfortable and Reliable Multimodal Health Monitoring, Adv. Funct. Mater. 32 (2022) 2200961, https://doi.org/10.1002/adfm.202200961.

[68] Z. Yan, D. Xu, Z. Lin, P. Wang, B. Cao, H. Ren, F. Song, C. Wan, L. Wang, J. Zhou, X. Zhao, J. Chen, Y. Huang, X. Duan, Highly stretchable van der Waals thin films for adaptable and breathable electronic membranes, Science 375 (2022) 852-859, https://doi.org/10.1126/science.abl8941.

Authors Biographies

Jiancheng Dong is a Ph.D. student in the School of Chemical and Material Engineering of Jiangnan University. He received his Bachelor and Master degrees in the School of Textile Science and Engineering of Jiangnan University. His current research interests focus on multifunctional textile-based electronics.

Xinwei Tang is a Ph.D. student in the School of Chemical and Material Engineering of Jiangnan University. He obtained his bachelor's degree from the College of Materials Science and Engineering, Qilu University of Technology in 2020. His current research interests focus on electromagnetic protection materials.

Yidong Peng is currently a Master student in the School of Chemical and Material Engineering of Jiangnan University, he obtained his bachelor's degree from College of Materials Science and Engineering, Southwest Jiaotong University in 2021. His research interest focuses on strain sensors and smart fabrics.

Chonghui Fan is a Ph.D. candidate in the College of Textile Science and Engineering of Jiangnan University. He received his Master degrees in the Jiangnan University. His current research interests focus on energy harvesting and wearable fiber-based sensors.

Le Li is a post-doctor of Jiangnan University. He received his PhD degree from Donghua University in 2020. His research interests include high-performance conducting polymer gel materials and additive manufacturing technology.

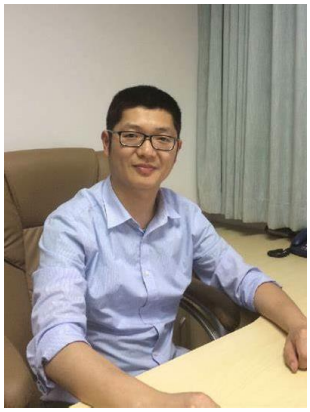

Chao Zhang is a professor of Donghua University. He received his PhD degree from Fudan University in 2013. His research interests include nano-/micro-fabrication of polymer composites for sensing and thermal management applications.

Feili Lai received his B.S. degree from Donghua University (2014), master degree from Fudan University (2017), and Ph.D. degree from Max Planck Institute of Colloids and Interfaces/Universität Potsdam (2019). He is now a research fellow of the Department of Chemistry, KU Leuven. His current interests include the design and synthesis of low-dimensional solids for energy storage and conversion applications, smart poly-gels, and the theoretical calculations.

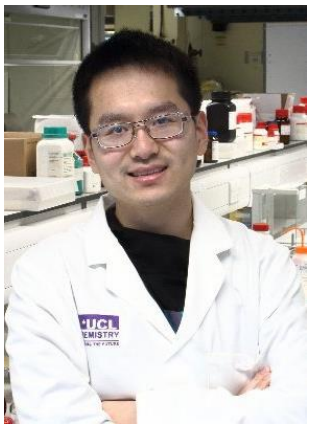

Guanjie He is Senior Lecturer at Queen Mary University of London. Dr. He received Ph.D. degree in Chemistry, University College London. Dr. He's research focuses on materials design for electrochemical energy storage and conversion applications.

Piming Ma received his bachelor, master and PhD degrees from South China University of Technology, Shanghai Jiaotong University, and Eindhoven University of Technology, respectively, and is currently a full-time professor in Jiangnan University. He is the leader of research group of Bio-polymer and Composites, and an editorial board member of Polymer Degradation and Stability.

Zicheng Wang received his bachelor, master and PhD degrees from University of Electronic Science and Technology of China, and is currently a full-time associate professor in Jiangnan University. His research focuses on functional nanocomposites for electromagnetic wave absorption/shielding.

Qufu Wei is a professor of Textile Science and Engineering in the School of Textiles and Clothing at Jiangnan University. He received his PhD degree from Heriot-Watt University in the UK. He currently serves as Director of the Key Laboratory of Eco-textiles within the Ministry of Education of P. R. China at Jiangnan University. His research interests lie in functional nanofibers, technical textiles and smart textiles.

Xiu-Ping Yan is a professor of chemistry at the School of Food Science and Technology, Jiangnan University, China. His research interests mainly focus on hyphenated techniques and advanced materials for analytical chemistry, biomedical science and food safety. He graduated in chemical education from Taizhou University, China (1981), received his M.S. in analytical chemistry from Dalian Institute of Chemical Physics, China (1987), and Ph.D. in environmental chemistry from the Re-search Center for Eco-Environmental Sciences, Chinese Academy of Sciences (1993).

Hai-Long Qian is an associate professor at the School of Food Science and Technology, Jiangnan University, China. His main research interests include the development of advanced porous materials for sample pretreatment and chromatography analysis of food and environmental samples. He received his B.S. from Anhui Science and Technology University (2011), M.S. from Tianjin University of Science & Technology (2014), and Ph.D. from Nankai University (2017), China.

Yunpeng Huang is currently an associate professor of the School of Chemical and Material Engineering, Jiangnan University. He received his PhD degree in polymer chemistry and physics from Fudan University in 2016. His research mainly focuses on the development of functional nanofibers and nanofiber composites.

Tianxi Liu is a professor of the School of Chemical and Material Engineering, Jiangnan University. He received his PhD degree from Changchun Institute of Applied Chemistry, Chinese Academy of Sciences in 1998. His research interests include polymer nanocomposites, polymer aerogel composites, nanofibers and their composites, new energy materials.

CRediT authorship contribution statement

Jiancheng Dong: Methodology, investigation, draft preparation; **Xinwei Tang**: Investigation, Data curation; **Yidong Peng**: Investigation, Data curation; **Chonghui Fan**: Data curation, validation; **Le Li**: Data curation, validation; **Chao Zhang**: Validation, conceptualization; **Feili Lai**: conceptualization, reviewing and editing; **Guanjie He**: conceptualization, reviewing and editing; **Piming Ma**: reviewing and editing; **Zicheng Wang**: Data curation, Reviewing and editing; **Qufu Wei**: Reviewing and editing; **Xiu-Ping Yan**: Reviewing and editing; **Hai-Long Qian**: Reviewing and editing; **Yunpeng Huang**: Data curation, validation, supervision, conceptualization, reviewing and editing; **Tianxi Liu**: Conceptualization, methodology, supervision, reviewing and editing

Declaration of Competing Interest

☒ The authors declare that they have no known competing financial interests or personal relationships that could have appeared to influence the work reported in this paper.

Graphical abstract

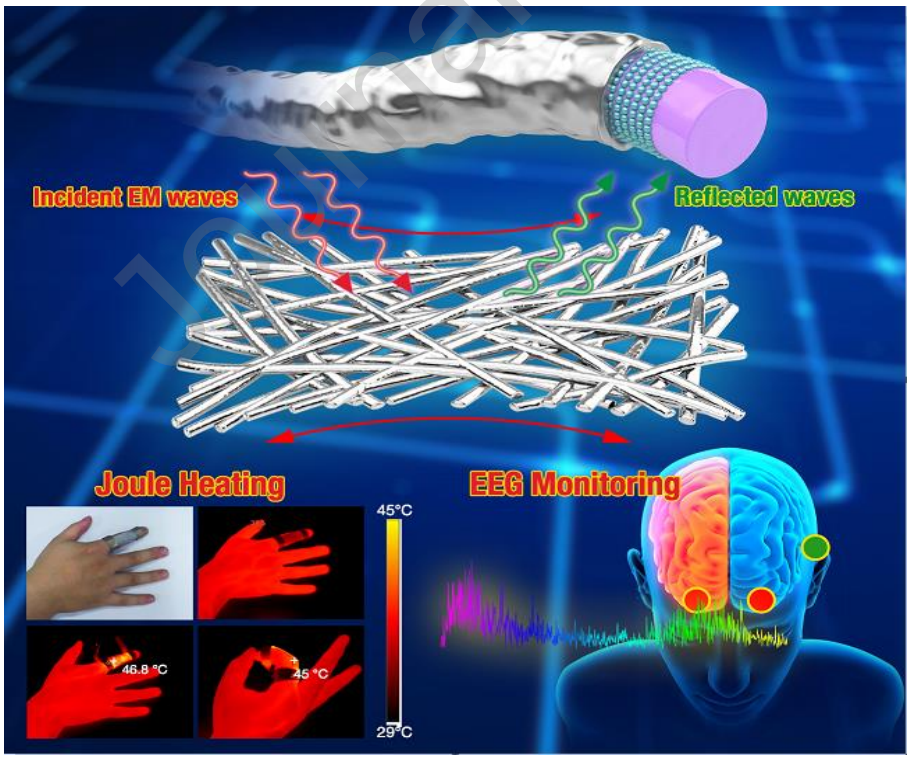

Highlights

- The electronic textile has superlyophilicity to liquid metal due to the fast alloying
- monolithic stretch activation is used to recover the breathability of liquid metal textile
- obtained electronic textile has a high conductivity upon 1000% elongation
- the electronic textile shows efficient EMI shielding and Joule heating performance
- the electronic textile can monitor human biophysical and bioelectrical signals